Suzaku View of Thermal Supernova Remnants

Satoru Katsuda[1]

[1]Code 662, NASA Goddard Space Flight Center, Greenbelt, MD 20771, U.S.A.
E-mail(SK): satoru.katsuda@nasa.gov

Abstract

The X-ray Imaging Spectrometer (XIS) onboard Suzaku is characterized by three major advantages: low and stable background, good response in low energies, and superior energy resolution. Utilizing these advantages, the XIS has attacked a number of supernova remnants (SNRs). The first advantageous point allows us to detect Fe, Mn, and Cr lines from young SNRs, while the second one reveals C and N lines from evolved SNRs. The third one enables us to detect line broadening due to either the Doppler effect, the thermal Doppler effect, or the ionization-timescale variation of several plasma components. For largely extended evolved SNRs, by combining the three advantages, spatially-resolved spectral analyses show us their metal distributions in unprecedented details. I will review such a Suzaku view of thermal SNRs.

Key words: ISM: abundances — supernova remnants

1. Introduction

After the launch of the Suzaku satellite in July 2005 (Mitsuda et al. 2007), the X-ray Imaging Spectrometer (XIS; Koyama et al. 2007), which is one of the X-ray detectors onboard the satellite, has been successfully operated, and has observed a number of supernova remnants (SNRs). Suzaku has unique capabilities compared with the other currently operating X-ray observatories, i.e., Chandra and XMM-Newton. The performance of CCD cameras onboard the three X-ray observatories are summarized in Table 1, from which we can see that each observatory plays complementary roles. Chandra has far superior spatial resolution, and XMM-Newton has high throughput and a large field of view (FOV). On the other hand, Suzaku has three advantages: 1) a very low and stable background especially at high energies, 2) high energy resolution which is nearly at the theoretical limit for CCDs, and 3) significant sensitivity below 0.5 keV. Each of the three advantages has played a part in obtaining new results. These results for thermal emission from SNRs, which will be briefly reviewed in this article, are summarized as follows:

- Detection of lines above 4 keV
- Detection of line broadening
- Detection of lines below 0.5 keV
- Spatially-resolved spectral analysis

2. Young SNRs

Thermal emission from young SNRs comes dominantly from the high-temperature (>1 keV) SN ejecta heated by the reverse shock. Therefore, young SNRs are ideal targets to investigate the SN ejecta.

2.1. Detection of Lines above 4 keV

Relative abundances of trace elements, such as Cr to Mn, are sensitive to Type-Ia SN explosion mechanism (Iwamoto et al. 1999). Therefore, they should provide an important diagnostic for these explosions. However, detection of the lines from Cr and Mn, were previously reported only from W49B SNR with ASCA. The larger effective area of the XIS together with its low background allows us to detect these emission lines for many other SNRs. So far, these include Tycho's SNR, Kepler's SNR, and LMC SNR, N103B. The XIS spectrum from the entire Tycho's SNR is shown in Fig. 1 (Tamagawa et al. 2009). In addition to the strong Fe K blend, we can see several line features which are detected for the first time in this observation. Badenes et al. (2008) had noted a correlation between the Mn to Cr mass ratio in the SN ejecta and the progenitor metallicities. The correlation is particularly tight for Type-Ia SNe, and can be well described by a power-law function. Using the flux ratio of Mn and Cr K lines from Tycho's SNR, the mass ratio is calculated within 0.3 to 1.2. The progenitor metallicity is then derived to be within 0.02 to 0.1, which translated to 1 to 5 times the solar value. Sub-solar metallicities are therefore safely rejected.

Different interesting science is found in Vela Jr. Vela Jr. is a relatively new SNR discovered 11 yrs ago by the

Table 1. Performance of CCD cameras onboard Suzaku, Chandra, and XMM-Newton

	Suzaku (XIS)	Chandra (ACIS)	XMM-Newton (EPIC)
Background level (@5 keV, normalized at the XIS)	1	5	3
Energy resolution (eV @1 keV and 6 keV)	60 and 140	80 and 150	80 and 150
Bandpass (keV)	0.2–12	0.5–12	0.5–12
Spatial resolution (arcsec for half-power diameter)	120	0.5	15
Effective area (cm^2 @ 1.5 keV)	1100	500	2200
Field of view ($arcmin^2$)	320	290	660

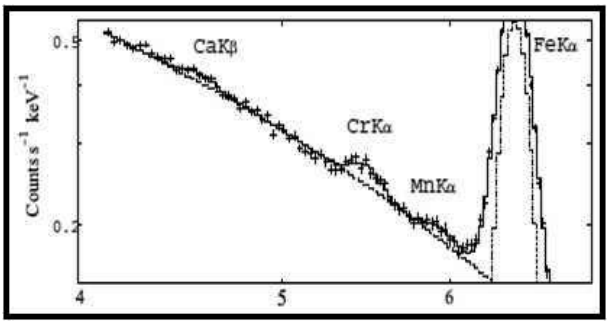

Fig. 1. XIS spectrum from Tycho's SNR (Tamagawa et al. 2009).

ROSAT all-sky survey (Aschenbach 1998). At the same time, gamma-ray emission lines from the decay chain of ^{44}Ti was reported (Iyudin et al. 1998). Because the decay time of ^{44}Ti is very short, Vela Jr. was inferred to be very young, most likely about 700 yrs old. Two years after the discovery, ASCA detected a possible line feature around 4 keV (Tsunemi et al. 2000), but only on the SIS0 chip (Slane et al. 2001). This line feature was attributed to K lines from Ca or Sc which are daughter elements of ^{44}Ti. It was also seen with XMM-Newton (Iyudin et al. 2005) and Chandra (Bamba et al. 2005). But later, the detection of gamma-ray emission was questioned by re-analysis of the same data. Therefore, the detection of line emission related to ^{44}Ti has been debated. In the meantime, Suzaku observed this remnant with the highest sensitivity at 4 keV (Hiraga et al. 2009). The XIS spectrum does not show any line features. Without evidence for ^{44}Ti, Vela Jr. turns out not to be as young as 700 yrs. An older age for this remnant is actually consistent with a recent claim based on the expansion measurement of the northwestern rim of the remnant (Katsuda et al. 2008a).

Also very interesting are strong radiative recombination continua (RRC) detected from IC443 (Yamaguchi et al. 2009). The ionization temperature determined from the intensity ratios of the RRC to He-like Kα line are clearly higher than the electron temperature determined from the width of the RRC. This is firm evidence for an extremely-overionized (recombinating) plasma. Such strong RRC were also detected from W49B SNR (Ozawa et al. 2009).

In SN1006, strong Fe K line emission was firmly detected for the first time (Yamaguchi et al. 2008). The detection of Fe K line is especially important, since it allows the elemental abundance of Fe to be measured. It finally confirmed that SN1006 is a remnant of a Type-Ia SN explosion. In RCW86, the spatial distribution of the Fe K line was revealed for the first time (Ueno et al. 2007; Yamaguchi et al. 2008).

2.2. Detection of Line Broadening

Detections of line broadening from young ejecta-dominated SNRs were made possible by XIS' high energy resolution. The causes of the line broadening found by the XIS are either multiple red and blue shifted lines, or thermal Doppler effects, or ionization effects.

Furuzawa et al. (2009) found the broadened Fe K line in Tycho's SNR. The authors also noticed that the center energy of the Fe K line stays constant with radius, while the widths significantly reduces toward the outer region. The broadened line from the central region clearly requires at least two lines. There are two possible interpretations on these two lines: one is that two plasmas with different ionization states emit each line, and the other is an expanding shell which produces red and blue shifted lines. The authors compared the radial variation of the line center energy and line widths with the two models. Since the expanding shell model better fits the data, the authors concluded that the line broadening is due to Doppler effects. The velocity of the expanding shell was derived to be about 3,000 km sec^{-1}. More recently, Hayato et al. (2009) expanded the analyses for inter-mediate mass elements (i.e., Si, S, Ar, and Ca). They found that all the lines are broadened and obtained the expansion velocity for Si and S to be $\sim$3,500 km sec^{-1}. This velocity is significantly higher than that of Fe. This is evidence for the fact that the onion-skin-like structure of the ejecta still retains in Tycho's SNR.

Broadened emission lines for Si and S K lines were also found in SN1006 (Yamaguchi et al. 2008). The authors

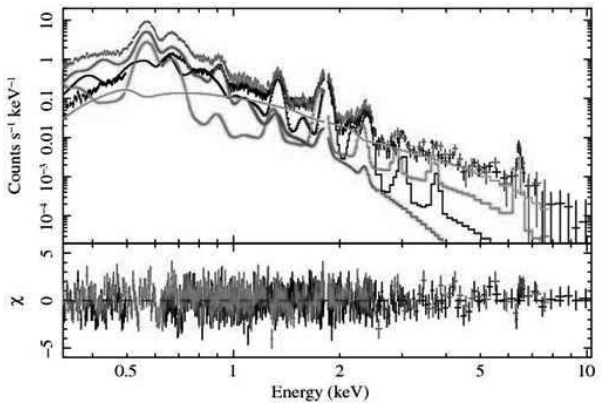

Fig. 2. XIS spectra (black and gray for front- and back-side illuminated CCD data, respectively) from the SE portion of SN1006 (Yamaguchi et al. 2008). The model consists of four components representing the ISM, two ejecta with different ionization ages, and nonthermal emission.

successfully modeled the thermal emission with an interstellar medium (ISM) component plus two ejecta components having different ionization ages. The XIS spectra extracted from the southeastern portion of SN1006 are shown in Fig. 2 along with the best-fit model. The ejecta component responsible for Fe K line emission has a very low ionization time scale. This suggests that the reverse shock has reached Si, S, and Fe rich ejecta very recently in this region.

N103B also shows significantly broadened line for Fe K (Yamaguchi et al. 2009). In this case, the main cause of the broadening is likely thermal Doppler effects rather than the other effects seen in Tycho's SNR or SN1006.

3. Evolved SNRs

In evolved SNRs, thermal emission originates from relatively low-temperature (< 1 keV) plasma which is a combination of the swept-up ISM and the ejecta. We can study both the ISM and the ejecta from evolved SNRs.

3.1. Detection of Lines below 0.5 keV

Since the plasma temperature of evolved SNRs are generally as low as < 1 keV, the thermal emission is dominated by line emission from light elements (i.e., C, N, O, Ne, and Mg). From these plasmas, C and N K lines can be clearly detected thanks to the good response of the XIS in the low energy bands below 0.5 keV. However, due to severe interstellar absorption at these energies, there are actually a few candidates from which we can detect these emission lines. Figure 3 shows an XIS spectrum extracted from the bright northeastern rim of the Cygnus Loop, in which we can clearly see emission lines from highly ionized C and N K lines for the first time (Miyata et al. 2007). Previous X-ray spectral analysis was performed assuming the same abundance among C, N, and O. Now, in the Suzaku era, we no longer have to assume these abundances. The spectral analysis showed that all the metal abundances were strongly depleted, typically 0.2 times the solar value. While the low abundance clearly shows that the origin of the plasma there is the ISM rather than the ejecta, such a strong depletion is not expected in the ISM around the Cygnus Loop. Miyata et al. (2008) investigated the effect of resonance line scattering as a possible explanation for the depletion. They estimated that O He-like K line could be reduced to 70% of its original strength. But, this does not fully explain the strongly depleted abundances observed. The strong depletion still remains an open question.

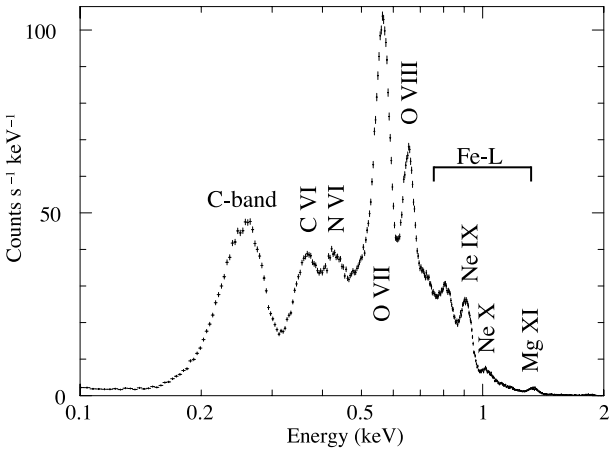

Fig. 3. XIS spectrum from the northeastern portion of the Cygnus Loop (Miyata et al. 2007).

3.2. Detailed Spatially-Resolved Spectral Analysis

Detailed spatial analysis for large SNRs is possible due to Suzaku's relatively large FOV plus the high effective area. Here, I will focus on Puppis A and the Cygnus Loop among the several other results published, i.e., North Polar Spur (Miller et al. 2008), the Vela SNR (Yamaguchi et al. 2009c), and G156.2+5.7 (Katsuda et al. 2009).

The middle-aged SNR Puppis A is one of the brightest SNRs in the X-ray sky. Suzaku observed the eastern part of this remnant (Hwang et al. 2008). The authors performed detailed spatially-resolved spectral analysis, and revealed abundance variations in this remnant. They noticed a region in the remnant with strongly enhanced abundances. Since the abundances there are above the solar values, this is clear evidence for the presence of the ejecta in this 4,000-yrs-old remnant. More recently, based on XMM-Newton archival data, we found a knotty feature partially coincident with the abundance-enhanced region (Katsuda et al. 2008b). Our spectral analysis of the knot showed super-solar metal abundances and blue-shifted lines. The line-of-sight velocity of the knot is estimated to be about 3,000 km sec^{-1}.

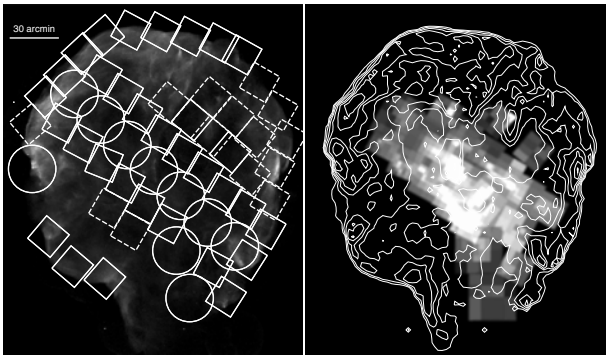

Fig. 4. *Left*: ROSAT HRI image of the Cygnus Loop with Suzaku XIS FOV (boxes) and XMM-Newton EPIC FOV (circles). The dashed boxes is Suzaku FOV to be observed during the AO4 cycle. *Right*: Ejecta distribution in the Cygnus Loop (Uchida et al. 2009b) revealed by detailed spatially resolved spectral analyses from Suzaku and XMM-Newton data.

Finally, I turn to the Cygnus Loop. So far, the Cygnus Loop had been observed in 32 pointings by Suzaku and 10 pointings by XMM-Newton. Figure 4 *left* shows these FOV (solid boxes for Suzaku and solid circles for XMM-Newton) as well as approved observations for the Suzaku AO4 cycle (dashed boxes) overlaid on the ROSAT HRI image of the entire Cygnus Loop. In total, the exposure times for Suzaku and XMM-Newton are about 800 ksec and 100 ksec, respectively. Previous ASCA observations revealed that the swept-up ISM is present in the rim regions, while the ejecta occupy the inside of the Loop. The XIS spectra extracted from the rim region and the central region show clear difference, and we confirmed this picture from our spectral analysis. To study both the ISM and the ejecta in detail, we have performed a detailed spatially-resolved spectral analysis, by dividing the FOV.

We generated abundance maps for the rim regions, and found that most of the rim regions show strongly depleted metal abundances similar to that seen in the northeastern rim region (only about 0.2 times the solar values: e.g., Miyata et al. 2007). However, on the other hand, we also found normal ($\sim$0.5 times the solar) abundance regions in the northern outermost rim region (Katsuda et al. 2008c; Uchida et al. 2009a). Another normal abundance region was also found in the southeastern rim (Tsunemi et al. 2009). Although the reason for the strong depletion of the ISM abundance seen in the most of the rim regions is not yet understood, we believe that this abundance inhomogeneity will be a key point to resolve this issue.

Figure 4 *right* shows the emission measure map of the Si ejecta (Tsunemi et al. 2007; Katsuda et al. 2008d; Kimura et al. 2009; Uchida et al. 2009b). We can see the centrally concentrated ejecta structure, which is evidence that the ejecta are not yet well-mixed with the ISM in this 10,000-yrs-old SNR. Also, we found that the ejecta distribution is shifted toward the south from the geometric center of the Loop. We proposed that this asymmetric ejecta distribution reflects the asymmetry of the supernova explosion itself.

4. Conclusion

The Suzaku XIS opened new windows for thermal emission from SNRs by its low background, high energy resolution, and good response at low energies. And, it has already yielded a number of completely new results for thermal emission from SNRs. Thus, thermal SNRs are fairly suitable targets for the Suzaku XIS, and we surely will have much more new results from future observations as well as existing data.

References

Aschenbach B. et al. 1998, Nature, 396, 141
Badenes C. et al. 2008, ApJ., 680, L33
Bamba A. et al. 2005, ApJ. 632, 294
Furuzawa A. et al. 2009, ApJ., 693, L61
Hayato A. et al. 2009, in preparation.
Hiraga J. et al. 2009, PASJ., 61, 275
Hwang U. et al. 2008, ApJ., 676, 378
Iwamoto K. et al. 1999, ApJS., 125, 439
Iyudin A. F. et al. 1998, Nature, 396, 1412
Iyudin A. F. et al. 2005, A&A., 429, 225
Katsuda S. et al. 2008a, ApJ., 678, L35
Katsuda S. et al. 2008b, ApJ., 678, 297
Katsuda S. et al. 2008c, PASJ., 60, S115
Katsuda S. et al. 2008d, PASJ., 60, S107
Katsuda S. et al. 2009, PASJ., 61, S155
Koyama K. et al. 2007, PASJ., 59, S23
Kimura M. et al. 2009, PASJ., 61, S137
Miller, E. et al. 2008, PASJ., 60, S95
Mitsuda K. et al. 2007, PASJ., 59, S1
Miyata E. et al. 2007, PASJ., 59, S163
Miyata E. et al. 2008, PASJ., 60, 521
Ozawa M. et al. 2009, in preparation
Yamaguchi H. et al. 2008a, PASJ., 60, S141
Yamaguchi H. et al. 2008b, PASJ., 60, S123
Yamaguchi H. et al. 2009a, submitted to ApJ.
Yamaguchi H. et al. 2009b, in preparation
Yamaguchi H. et al. 2009c, ApJ., 696, 1548
Slane P. O. et al. 2001, ApJ., 548, 814
Tamagawa T. et al. 2009 PASJ., 61, S167
Tsunemi H. et al. 2000, PASJ., 52, 887
Tsunemi H. et al. 2007, ApJ., 671, 1717
Tsunemi H. et al. 2009, PASJ., 61, S147
Ueno M. et al. 2007, PASJ., 59, S171
Uchida H. et al. 2009a, PASJ., 61, 301
Uchida H. et al. 2009b, PASJ., 61, 503